Supporting Information for

# A Freestanding Cellulose Nanofibril–Reduced Graphene Oxide–Molybdenum Oxynitride Aerogel Film Electrode for All-Solid-State Supercapacitors with Ultrahigh Energy Density

Qifeng Zheng,[ab] Alexander Kvit,[c] Zhiyong Cai,[d] Zhenqiang Ma,[e] and Shaoqin Gong*[abf]

[a] *Department of Material Science and Engineering, University of Wisconsin–Madison, WI 53706, USA.*

[b] *Wisconsin Institute for Discovery, University of Wisconsin–Madison, WI 53715, USA*

[c] *Materials Science Center, University of Wisconsin–Madison, Madison, WI 53706, USA*

[d] *Forest Product Laboratory, USDA, Madison, WI 53726, USA*

[e] *Department of Electrical Engineering, University of Wisconsin–Madison, WI 53706, USA*

[f] *Department of Biomedical Engineering, University of Wisconsin–Madison, WI 53706, USA*

*Email: shaoqingong@wisc.edu; Tel: +01 6083164311.*

**Supplementary Video S1**: Charging the CNF/RGO/$MoO_xN_y$ aerogel film-based all-solid-state supercapacitor by porous CNF/PDMS film-based nanogenerators (NG), the NG-charged solid-state supercapcitor can easily light up an LED light.

**Supplementary Video S2**: One single supercapacitor device can light the LED very well for about four hours.

**Supplementary Experimental Details**

**Materials:** Molybdenum powder (99.5 wt.%, ~170 mesh), hydrazine monohydrate (98 wt.%), and 1-butyl-1-methylpyrrolidinium bis(trifluoromethylsulfonyl)imide ([BMPY][$NTf_2$]) were purchased from Alfa Aesar. 2,2,6,6-tetramethyl-1-piperidinyloxy (TEMPO, 98 wt.%), potassium permanganate (99 wt.%), hydrogen peroxide solution (30 wt.%), sulfuric acid (98 wt.%), poly(vinyl alcohol) (PVA, $M_w$: 89 kDa–98 kDa), and poly(vinylidene fluoride) (PVDF, average Mw ~534 kDa) were obtained from Sigma–Aldrich. Poloxamer 407 (P407, a poly (ethylene glycol)-b-poly(propylene glycol)-b-poly(ethylene glycol) triblock copolymer) was kindly provide by BASF Corporation (Tarrytown, NY). Sodium chlorite, sodium hypochlorite solution, sodium bromide, phosphoric acid, and other chemicals were of laboratory grade (Fisher Scientific, USA) and used without further purification.

**Preparation of Cellulose Nanofibrils (CNFs):** A commercially supplied, fully bleached eucalyptus Kraft pulp was used to prepare the CNFs by TEMPO-oxidation as previously reported.[1, 2] Briefly, fully bleached eucalyptus fibers were oxidized with sodium hypochlorite using TEMPO as a catalyst at a temperature of 60 °C for 48 h. The fibers were then thoroughly washed and refined in a disk refiner with a gap of approximately 200 μm. The coarse fibers were separated by centrifuging at 12,000 G, and the fine CNF dispersion was then concentrated using ultrafiltration. A final refining step was performed in which the nanofiber dispersion was passed through an M-110EH-30 microfluidizer (Microfluidics,

Newton, MA) once with 200 μm and 87 μm chambers in series. The resulting CNF suspension with a concentration of 0.85% was stored at 4 °C without any treatment before future utilization.

**Preparation of Graphene Oxide (GO):** Graphene oxide (GO) was prepared from purified natural graphite powder using an improved Hummer's method reported by Marcano.[2, 3] Briefly, graphite flakes (2.0 g) and KMnO4 (12.0 g) were slowly added into a mixture of concentrated $H_2SO_4$/$H_3PO_4$ (180 ml:20 ml) and then stirred at 50 °C for 12 h. Afterward, the mixture was cooled to room temperature and then poured onto a mixture of ice (~200 ml) with $H_2O_2$ solution (2 ml, 30 wt.%). The mixture was centrifuged (10,000 rpm for 15 min), and the supernatant was decanted. The remaining solid material was then washed in succession with water, 30% HCl, ethanol, and water. For each wash, the filtrate was centrifuged (10,000 rpm for 15 min) and the supernatant was decanted. The remaining solid was further purified by dialysis against DI water for 3 days. The solution after dialysis was freeze-dried for 24 h to obtain the GO (3.6 g).

**Preparation of Ultralong Molybdenum Trioxide Nanobelts ($MoO_3$):** The ultralong molybdenum trioxide was prepared using a modified hydrothermal method as previously reported.[4] To be specific, 1 g of molybdenum power was added into 10 mL deionized water to form a uniform dispersion via the aid of sonication. Afterward, 10 mL 30% (wt%) $H_2O_2$ was slowly added and the solution was continuously stirred for 30 min to react thoroughly. After being transferred to a Teflon-lined stainless steel autoclave, the resulting mixture was heated in a vacuum oven at 220 °C for 7 days. The precipitate was then filtered and washed with water and ethanol several times until the solution became clear. The solid material was freeze-dried for 24 h to obtain the $MoO_3$ (1.48 g).

**Electrochemical Characterization:** The electrochemical parameters were calculated as follows.[5, 6]

For the three-electrode system, the specific capacitances of the electrodes were calculated from their CV curve at different scan rates and galvanostatic charge–discharge curves at different current densities using Equation (S1) and (S2), respectively,

$$C_{s,M} = \frac{\int I \times dV}{v \times M_1 \times \Delta V} \tag{S1}$$

$$C_{s,M} = \frac{I \times \Delta t}{M_1 \times \Delta V} \tag{S2}$$

For solid-state supercapacitors, the specific capacitances of the electrodes were calculated based on the mass or area or volume from the galvanostatic charge–discharge curves at different current densities using the following equations.

$$C_{s,M} = 2 \times \frac{I \times \Delta t}{M_2 \times \Delta V} \tag{S3}$$

$$C_{s,S} = 2 \times \frac{I \times \Delta t}{S \times \Delta V} \tag{S4}$$

$$C_{s,V} = 2 \times \frac{I \times \Delta t}{V \times \Delta V} \tag{S5}$$

For solid-state supercapacitors, the specific capacitances of the electrodes can also be calculated based on the mass from CV curves at different scan rates using the following equation.

$$C_{s,M} = 2 \times \frac{\int I \times dV}{v \times M_2 \times \Delta V} \tag{S6}$$

The capacitance of a solid-state supercapacitor was calculated according to the following equations.

$$C_{device,M} = \frac{1}{4}C_{s,M} = \frac{1}{2} \times \frac{I \times \Delta t}{M_2 \times \Delta V} \quad \text{(S7)}$$

$$C_{device,S} = \frac{1}{2}C_{s,S} = \frac{I \times \Delta t}{S \times \Delta V} \quad \text{(S8)}$$

$$C_{device,V} = \frac{1}{4}C_{s,V} = \frac{1}{2} \times \frac{I \times \Delta t}{V \times \Delta V} \quad \text{(S9)}$$

The energy density and power density of the solid-state supercapacitor was calculated according to Equation (S10) and Equation (S11), respectively,

$$E_{device} = \frac{C_{device} \times (\Delta V)^2}{2 \times 3600} \quad \text{(S10)}$$

$$P_{device} = \frac{E_{device} \times 3600}{\Delta t} \quad \text{(S11)}$$

where $I$ is the applied current, $v$ is the scan rate, and $\Delta t$ is the discharge time of the galvanostatic charge/discharge curves, and $\Delta V$ is the operating voltage window from the discharge curve excluding the *IR* drop. $M_1$ *and* $M_2$ are the weight of a single electrode in the three-electrode system and symmetric two-electrode solid-state system, respectively. $S$ and $V$ are the area and volume of a single electrode in solid-state supercapacitor, respectively.

For the solid-state supercapacitors, the area made accessible to the electrolyte was 2.4 $cm^2$, corresponding to a mass of 6.0 mg of the active materials (RGO and $MoO_xN_y$) per electrode. The areal density and volumetric density of the active materials were calculated to be 2.5 $mg/cm^2$ and 165 $mg/cm^3$ per electrode, respectively.

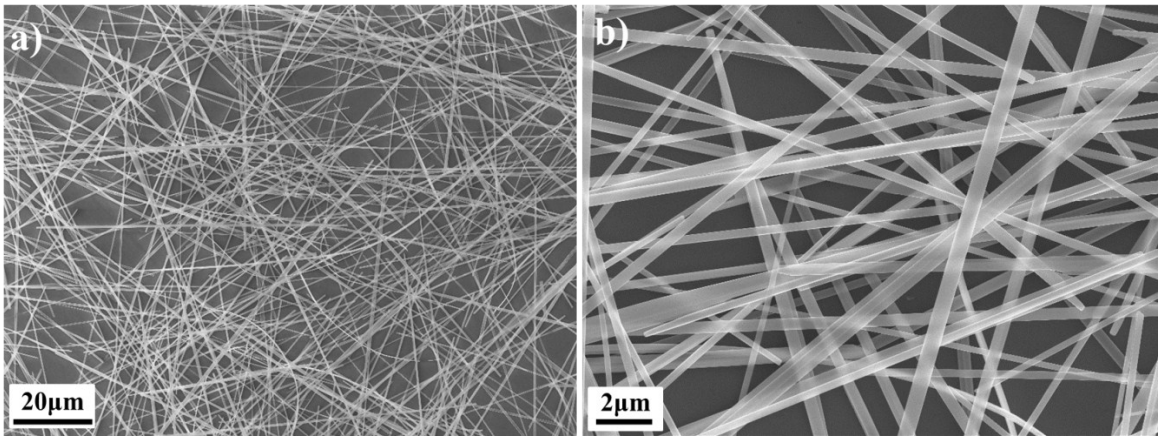


**Figure S1**. (a, b) SEM images of $MoO_3$ nanobelts.

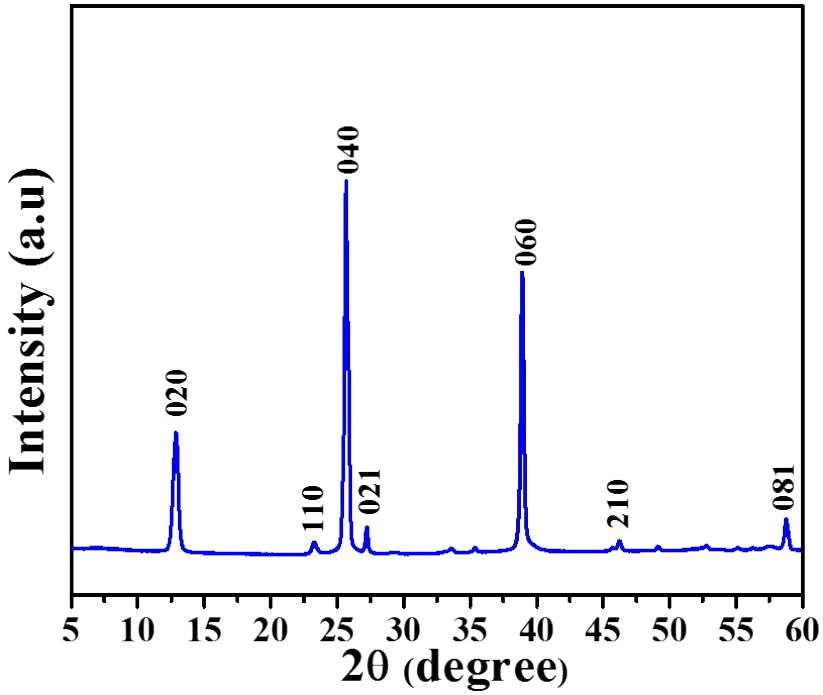


**Figure S2**. XRD patterns of $MoO_3$ nanobelts demonstrating an orthorhombic crystalline structure.

**Figure S3**. A digital image of the CNF/GO/$MoO_3$ aerogel sample with an ultra-light weight of 103 mg and a dimension of 5.5 cm in diameter and 0.7 cm in thickness.

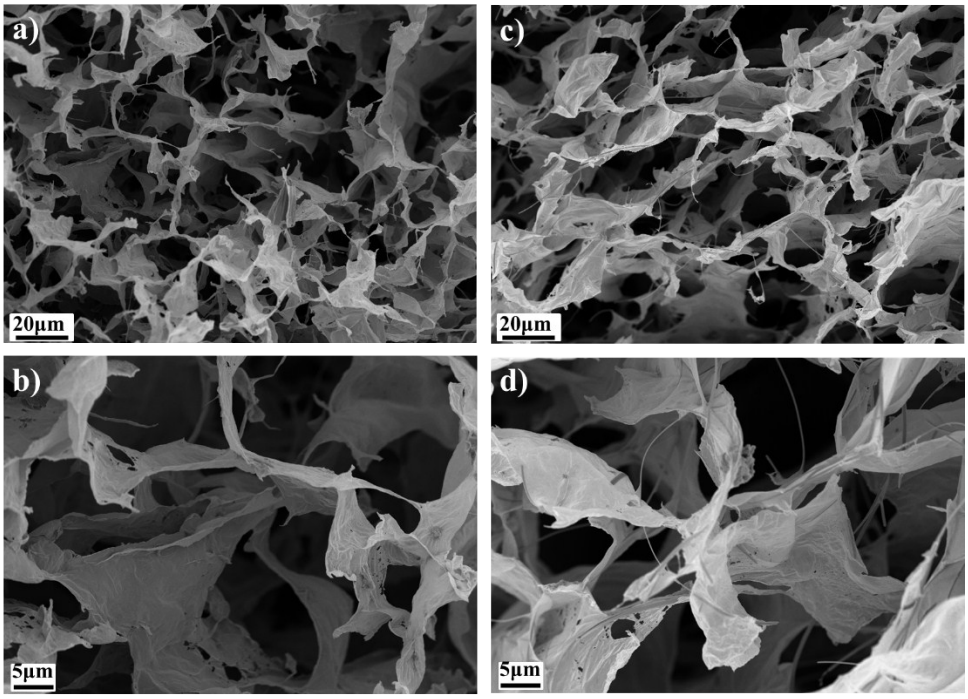


**Figure S4.** SEM images of the cryofractured surfaces of aerogels: (a, b) CNF/GO aerogel, and (c, d) CNF/GO/$MoO_3$ aerogel.

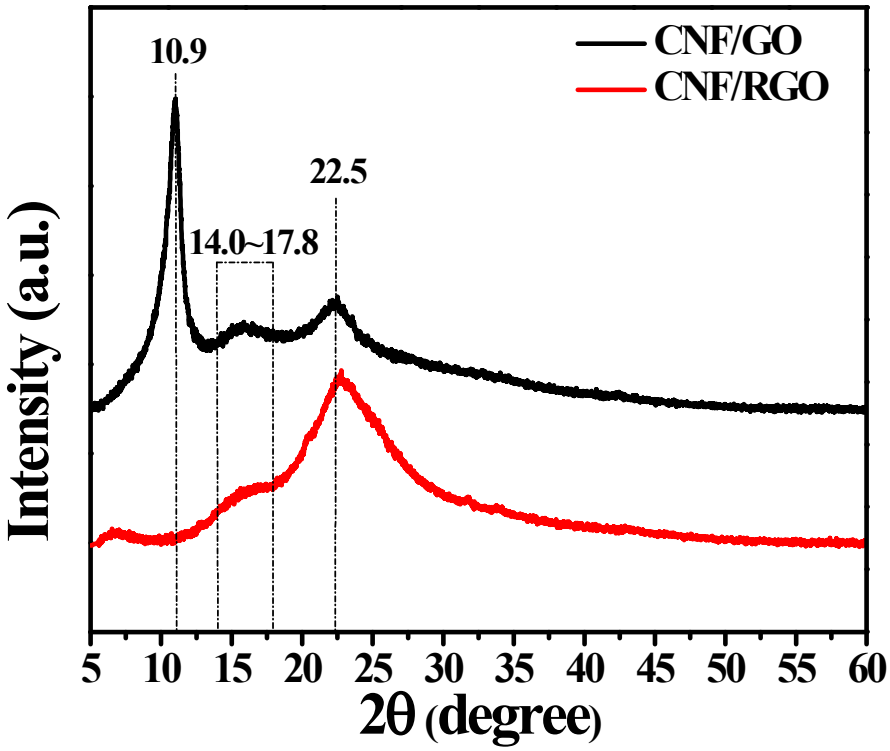


**Figure S5.** XRD patterns of the CNF/GO and CNF/RGO aerogel films.

In Figure S5, the diffaction peak at $2\theta$= 22.5° corresponded to the (002) lattice planes of the cellulose I crystalline structure, while the two overlapping peaks at $2\theta$= 14.0°–17.8° corresponded to the (101) and $(10\bar{1})$ lattice planes of the cellulose I crystalline structure.

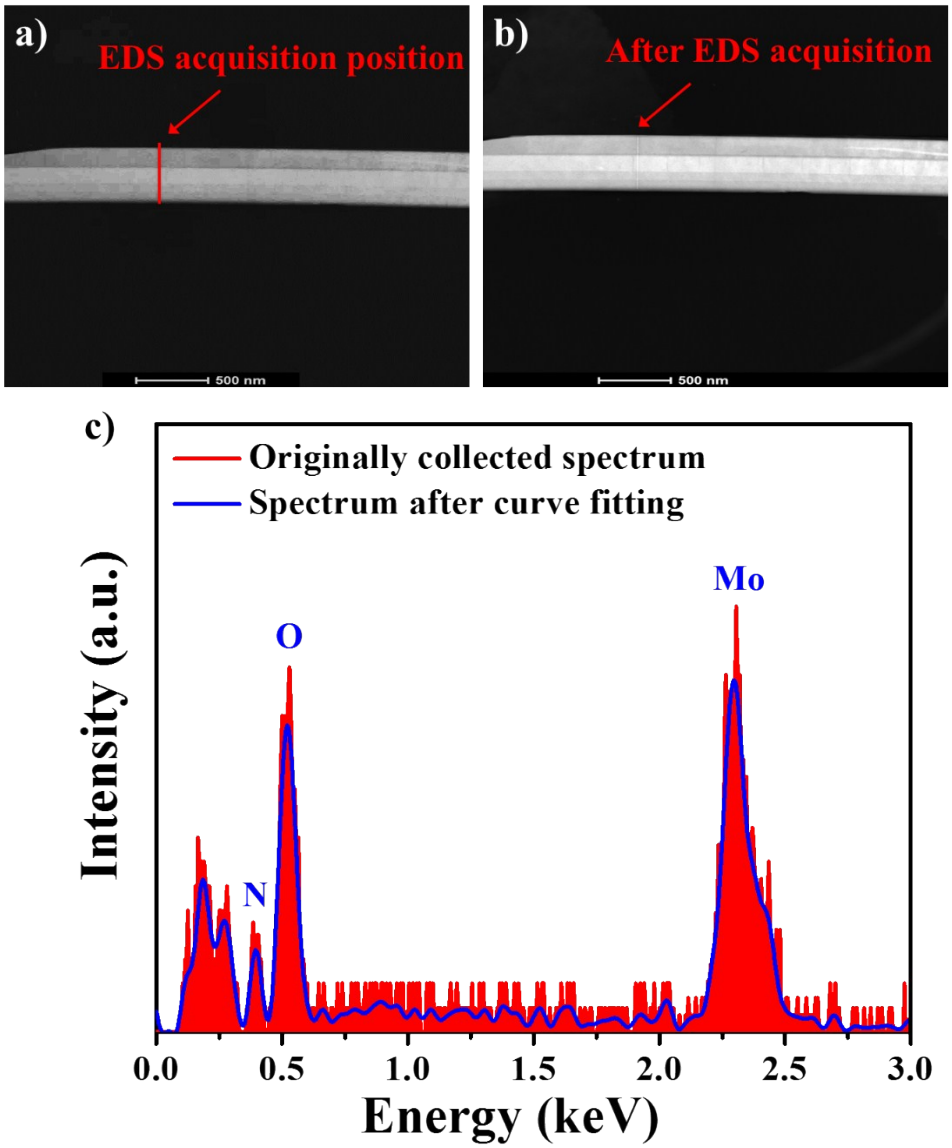


**Figure S6.** TEM EDS analysis of the $MoO_xN_y$ NBs: (a) EDS acquisition position, (b) the $MoO_xN_y$ NBs showed a clear damage line after EDS acquisition, and (c) EDS spectra.

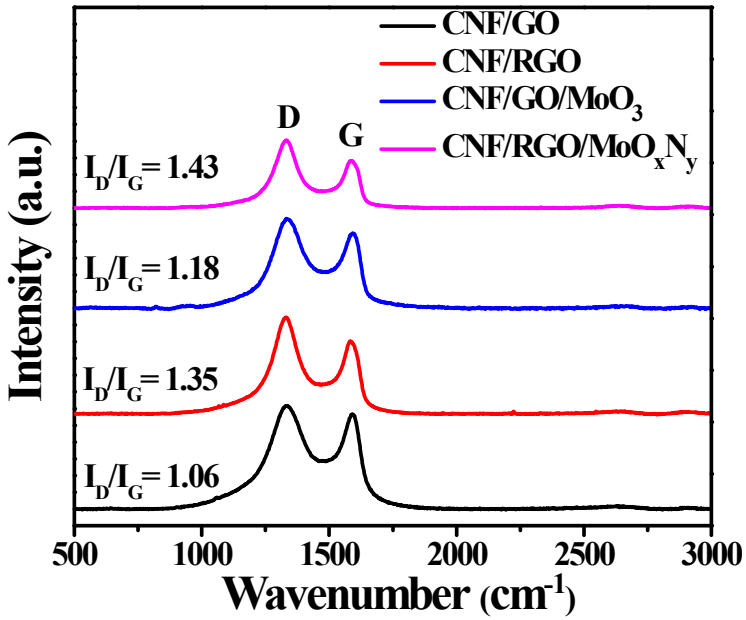


**Figure S7.** Raman spectra of the CNF/GO, CNF/RGO, CNF/GO/$MoO_3$, and CNF/RGO/$MoO_xN_y$ aerogel films.

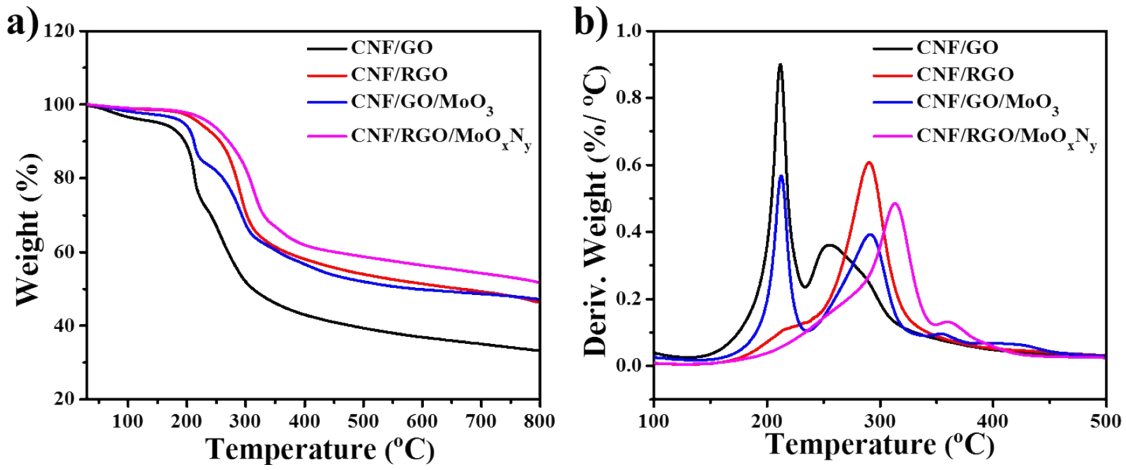


**Figure S8.** (a) TGA curves and (b) DTG curves of the CNF/GO, CNF/RGO, CNF/GO/$MoO_3$, and CNF/RGO/$MoO_xN_y$ aerogel films.

The thermal stabilities of the CNF/GO, CNF/RGO, CNF/GO/$MoO_3$, and CNF/RGO/$MoO_xN_y$ aerogel films were measured by a thermogravimetric analyzer (TGA) in nitrogen from 30 to 800 °C and are shown in Figure S8. As shown in Figure S8 (b), the CNF/GO and CNF/GO/$MoO_3$ aerogel films showed two major weight loss processes. The weight loss occurring in the temperature range of 150 to 230°C was attributed to the loss of oxygen-containing groups from the GO.[7] The weight loss occurring in the temperature range of 233 to 413°C corresponded to the decomposition of CNFs in the CNF/GO and CNF/GO/$MoO_3$ aerogel films, which was confirmed by direct comparison with the TGA curves of pure CNF aerogels.[1] There was only one major weight loss process shown in the TGA curves of the CNF/RGO and CNF/RGO/$MoO_xN_y$ aerogel films and it was attibuted to the decomposition of the CNFs. These results support the fact that GO was successfully reduced to RGO in both the CNF/GO and CNF/GO/$MoO_3$ aerogel films.

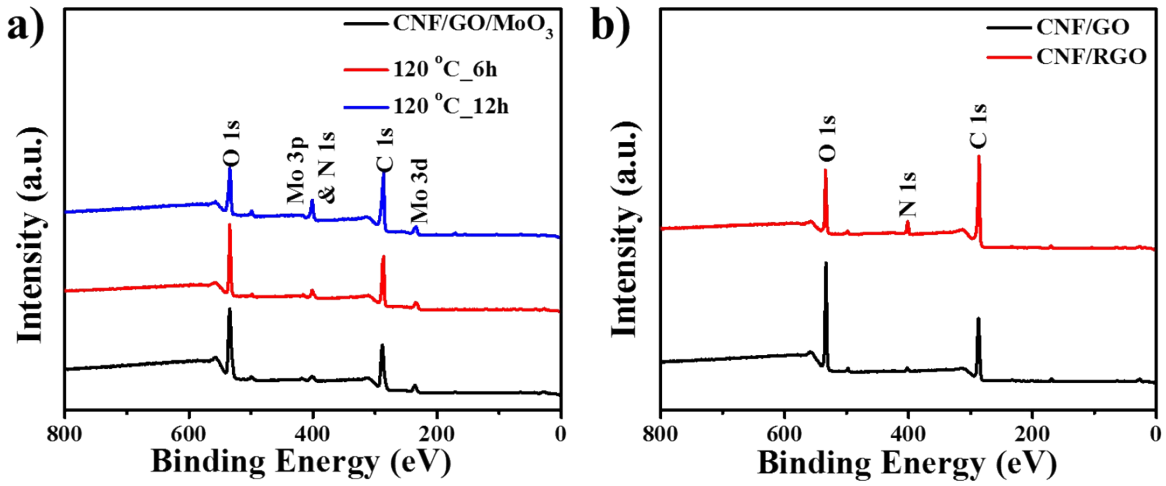


**Figure S9.** (a) XPS survey spectra of the pristine CNF/GO/$MoO_3$ aerogel film, and CNF/GO/$MoO_3$ aerogel film after either 6 or 12 h hydrazine reduction. (b) XPS survey spectra of the CNF/GO and CNF/RGO aerogel films.

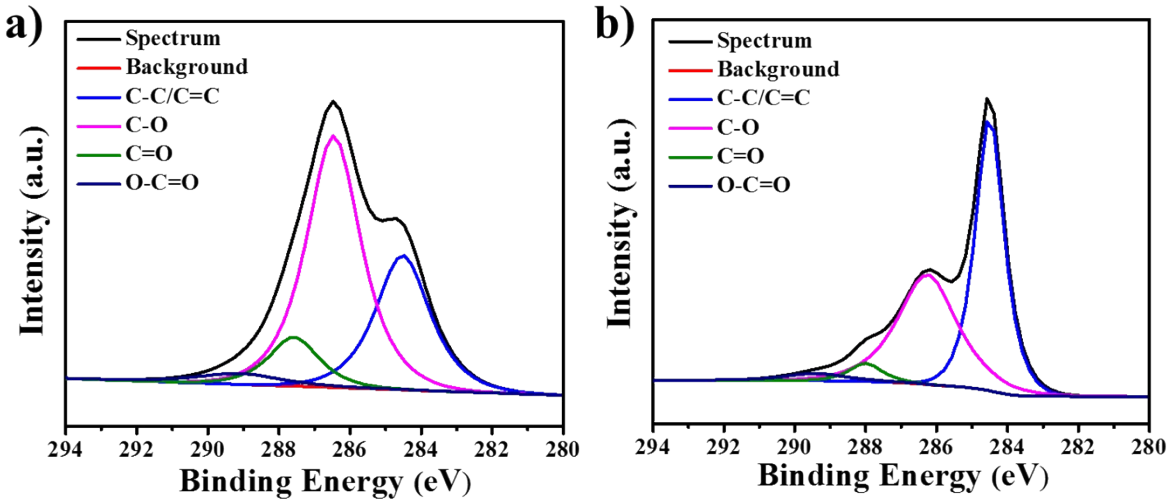


**Figure S10.** High-resolution C1s XPS spectra of the (a) CNF/GO aerogel film, and (b) CNF/RGO aerogel film.

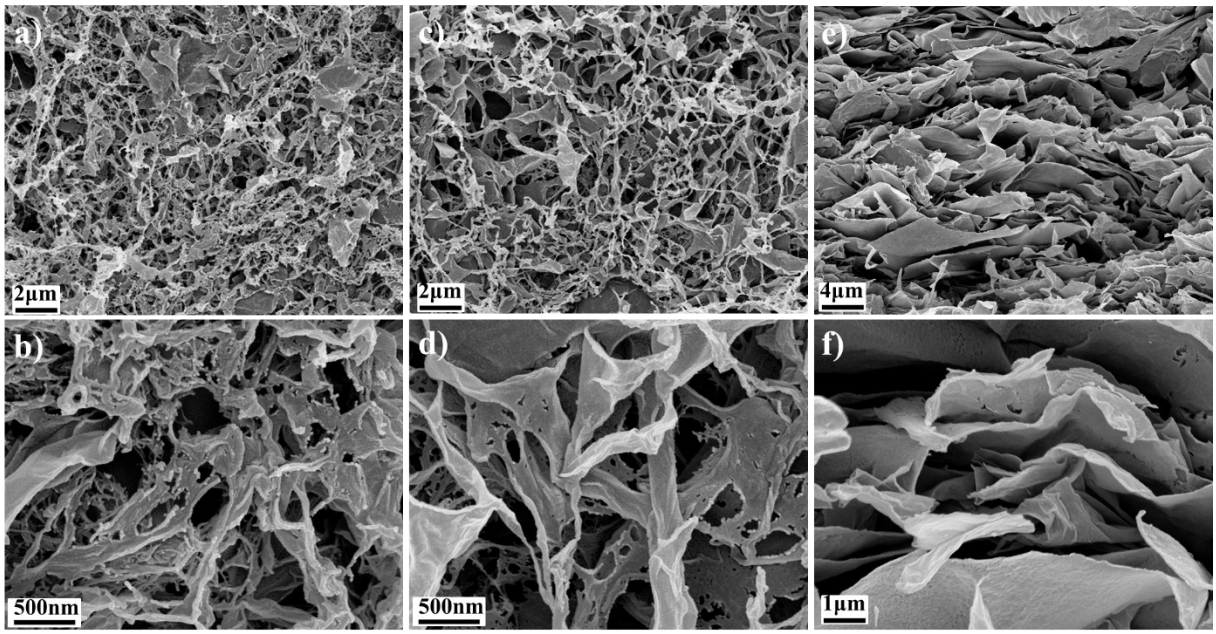


**Figure S11.** SEM images of the CNF/GO aerogel films: (a, b) the bottom surface of the aerogel film; SEM images of the CNF/RGO aerogel films: (c, d) the bottom surface of the aerogel film, and (e, f) a cross-section of the aerogel film.

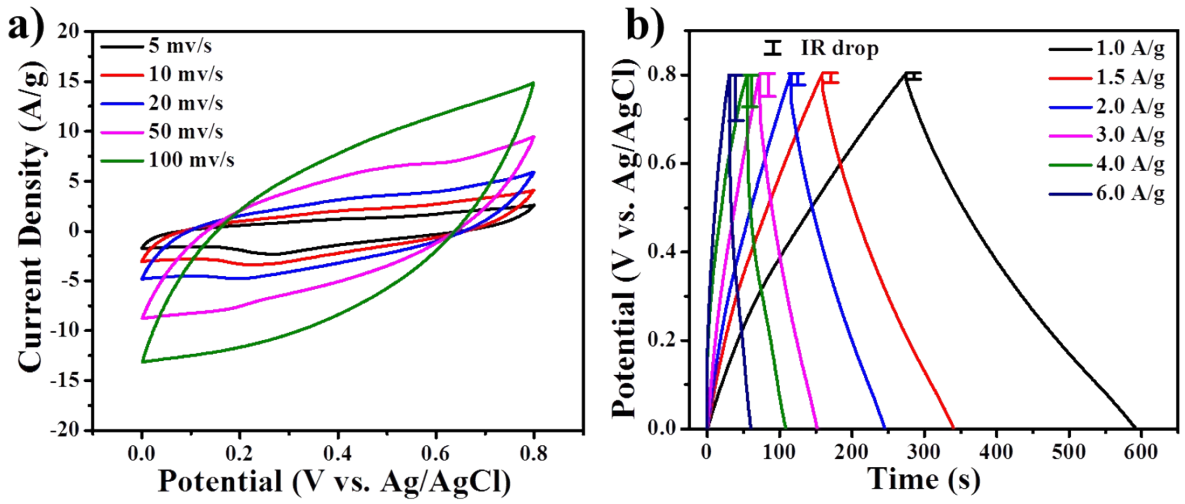


**Figure S12.** (a) CV curves of the CNF/RGO aerogel film electrode at different scan rates; and (b) galvanostatic charge–discharge curves of the CNF/RGO aerogel film electrodes at different current densities in 1.0 M $H_2SO_4$ aqueous electrolyte in a three-electrode system.

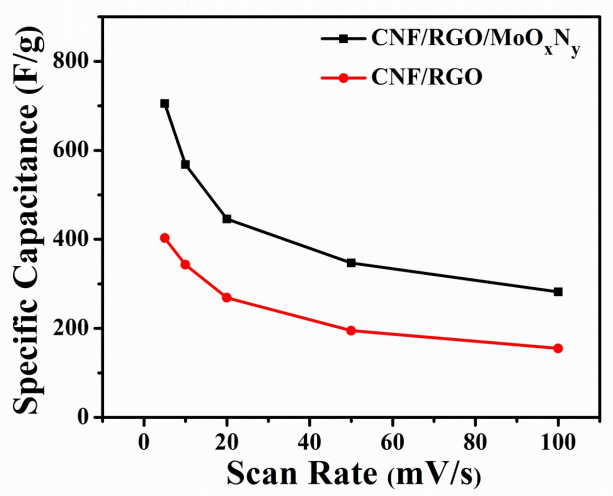


**Figure S13.** Specific capacitance of the CNF/RGO and CNF/RGO/$MoO_xN_y$ aerogel film electrodes as a function of scan rates in 1.0 M $H_2SO_4$ aqueous electrolyte in a three-electrode system.

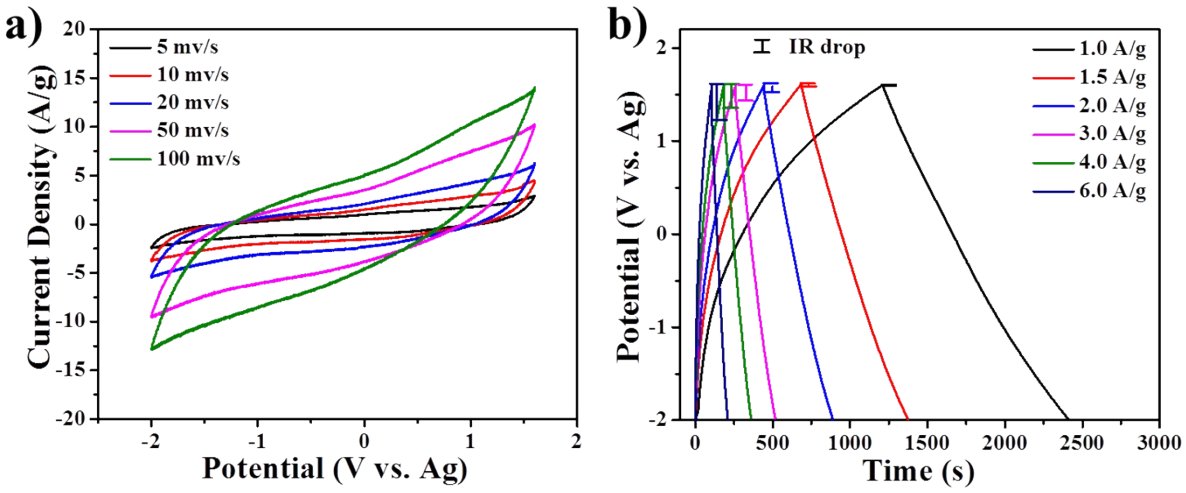


**Figure S14.** (a) CV curves of the CNF/RGO aerogel film electrode at different scan rates; and (b) galvanostatic charge–discharge curves of the CNF/RGO aerogel film electrodes at different current densities in 50 vol.% [BMPY][$NTf_2$] acetonitrile solution in a three-electrode system.

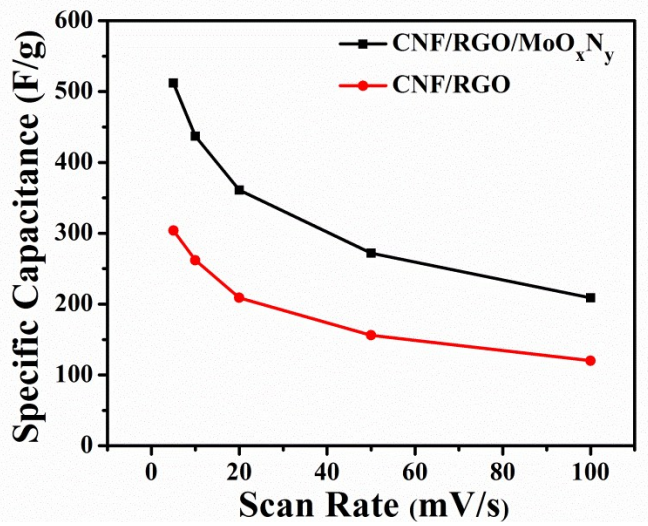


**Figure S15.** Specific capacitance of the CNF/RGO and CNF/RGO/$MoO_xN_y$ aerogel film electrodes as a function of scan rates in 50 vol.% [BMPY][$NTf_2$] acetonitrile solution in a three-electrode system.

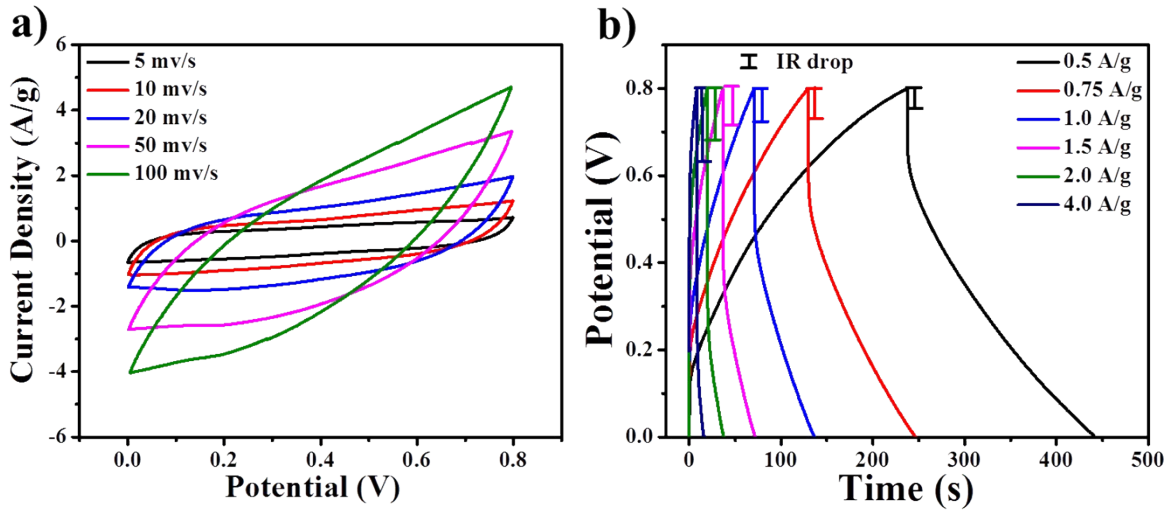


**Figure S16.** (a) CV curves and (b) galvanostatic charge–discharge curves of the CNF/RGO aerogel film-based solid-state supercapacitors employing PVA-$H_2SO_4$ hydrogel as the electrolyte.

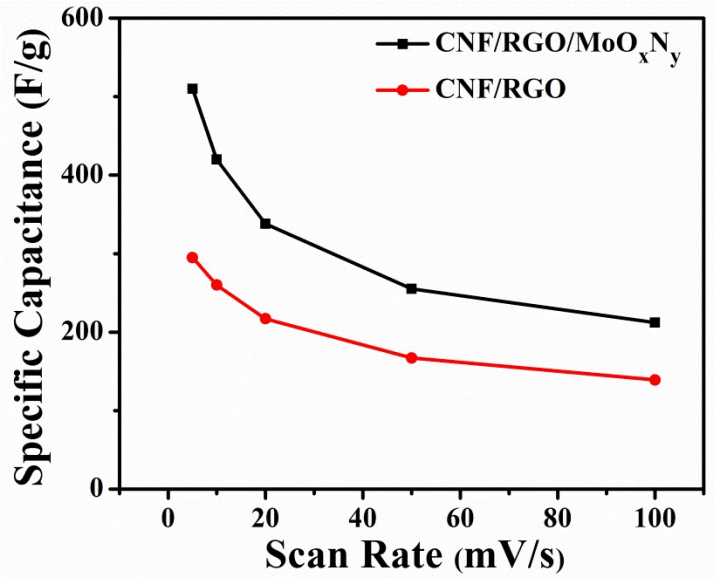


**Figure S17.** Specific capacitance of the CNF/RGO and CNF/RGO/$MoO_xN_y$ aerogel film-based all-solid-state supercapacitors employing PVA-$H_2SO_4$ hydrogel as the electrolyte at different scan rates.

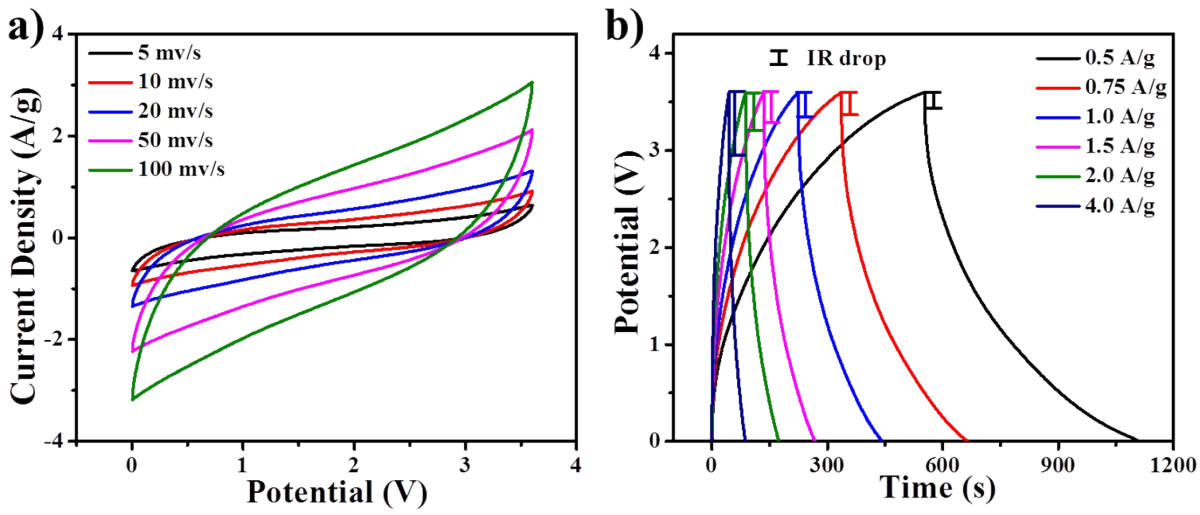


**Figure S18.** (a) CV curves and (b) galvanostatic charge–discharge curves of the CNF/RGO aerogel film-based solid-state supercapacitors employing PVDF-P407-[BMPY][$NTf_2$] ionogel as the electrolyte.

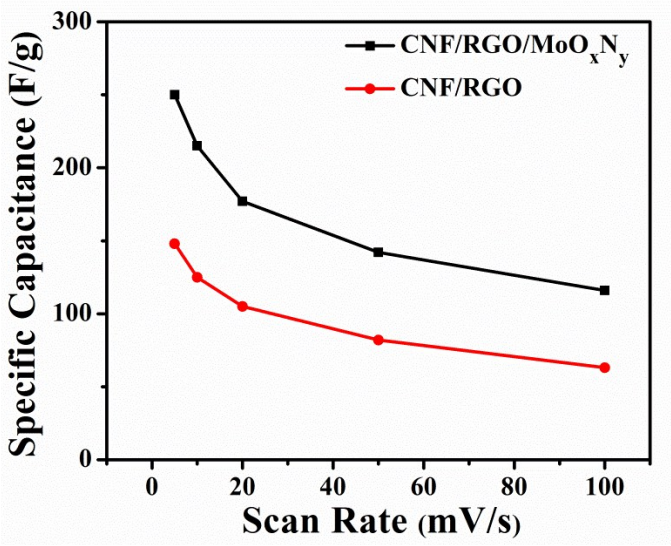


**Figure S19.** Specific capacitance of the CNF/RGO and CNF/RGO/$MoO_xN_y$ aerogel film-based all-solid-state supercapacitors employing PVDF-P407-[BMPY][$NTf_2$] ionogel as the electrolyte at different scan rates.

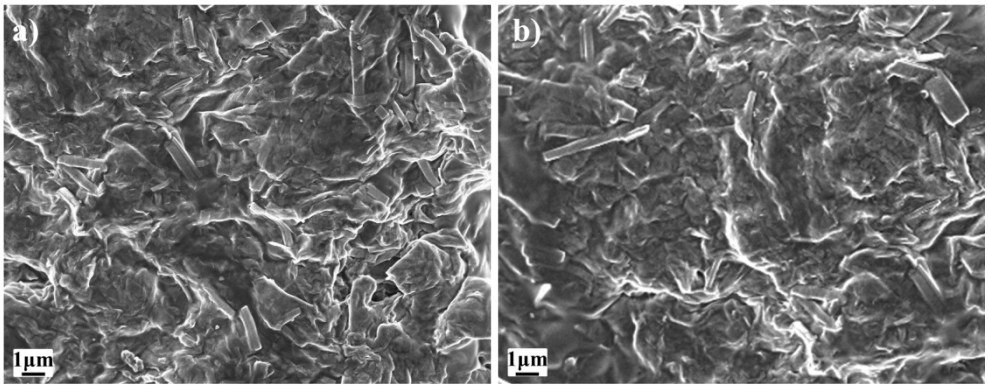


**Figure S20.** SEM image of the cross-section of the CNF/RGO/$MoO_xN_y$ aerogel electrode infiltrated with PVDF-P407-[BMPY][$NTf_2$] ionogel electrolyte: (a) before, and (b) after 2000 cyclic test.

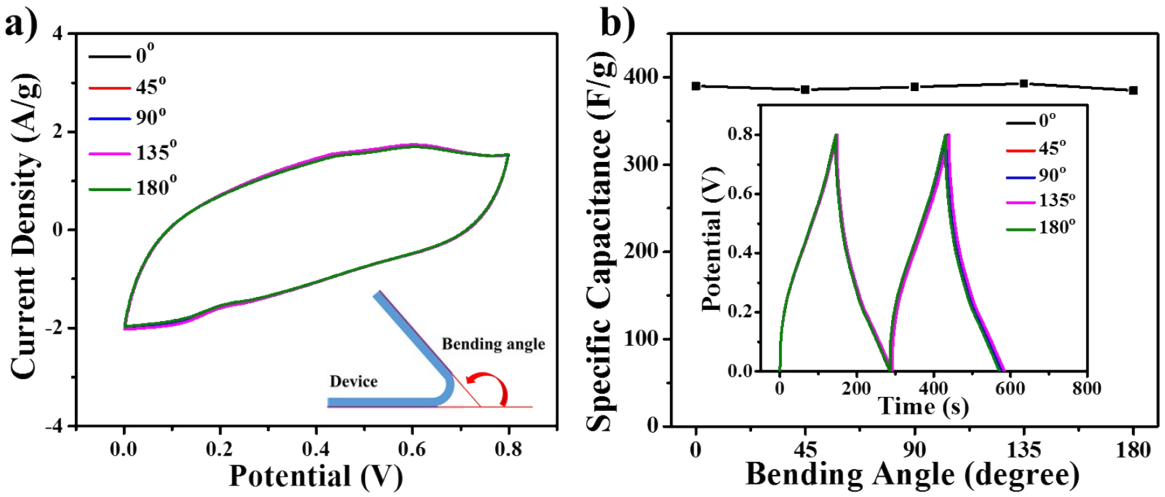


**Figure S21.** Flexibility tests of the CNF/RGO/$MoO_xN_y$-based solid-state supercapacitors employing PVA-$H_2SO_4$ hydrogel as the electrolyte. (a) Cyclic voltammetry curves of a supercapacitor at different bending angles with a scan rate of 10 mV/s. (b) Dependence of specific capacitance for a supercapacitor at different bending angles. The inset is charge–discharge curves of a supercapacitor at different bending angles with a current density of 1 A/g.

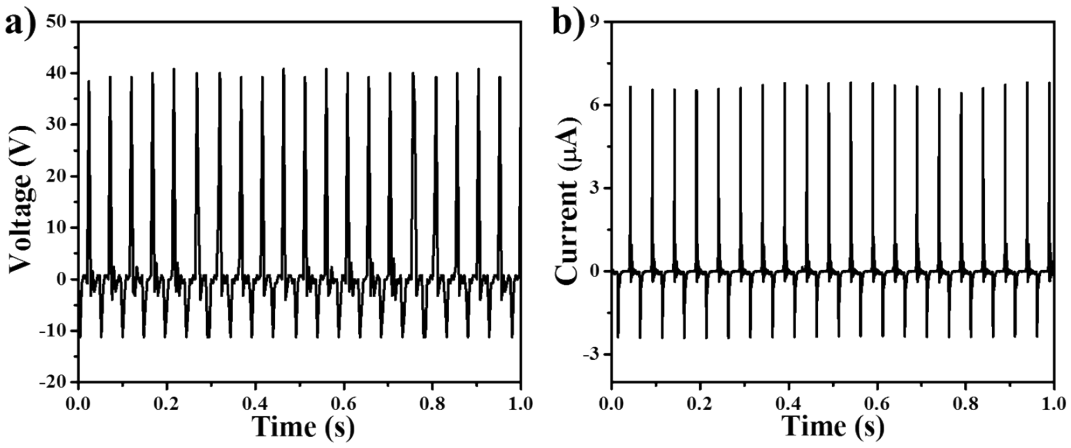


**Figure S22.** The electric output (a) voltage and (b) current measurement of the porous CNF/PDMS film-based NG under a compressive stress of 0.04 MPa at a frequency of 10 Hz.

**Reference:**


1. A. Javadi, Q. Zheng, F. Payen, A. Javadi, Y. Altin, Z. Cai, R. Sabo and S. Gong, *Acs Appl Mater Inter*, 2013, **5**, 5969-5975.
2. Q. Zheng, Z. Cai, Z. Ma and S. Gong, *Acs Appl Mater Inter*, 2015, **7**, 3263-3271.
3. D. C. Marcano, D. V. Kosynkin, J. M. Berlin, A. Sinitskii, Z. Sun, A. Slesarev, L. B. Alemany, W. Lu and J. M. Tour, *ACS Nano*, 2010, **4**, 4806-4814.
4. B. Yao, L. Huang, J. Zhang, X. Gao, J. Wu, Y. Cheng, X. Xiao, B. Wang, Y. Li and J. Zhou, *Adv Mater*, 2016, **28**, 6353-6358.
5. Y. Shao, M. F. El-Kady, C.-W. Lin, G. Zhu, K. L. Marsh, J. Y. Hwang, Q. Zhang, Y. Li, H. Wang and R. B. Kaner, *Adv Mater*, 2016, **28**, 6719-6726.
6. K. Zhou, W. Zhou, X. Liu, Y. Sang, S. Ji, W. Li, J. Lu, L. Li, W. Niu, H. Liu and S. Chen, *Nano Energy*, 2015, **12**, 510-520.
7. S. Stankovich, D. A. Dikin, R. D. Piner, K. A. Kohlhaas, A. Kleinhammes, Y. Jia, Y. Wu, S. T. Nguyen and R. S. Ruoff, *Carbon*, 2007, **45**, 1558-1565.